SUPPORTING INFORMATION

Nitrogen Fixation using Metallic Lithium Nanoparticles Formed by Electrospray Deposition

Dylan T. Holden,[a] Myles Q. Edwards,[a] Zhongxia Shang,[b] and R. Graham Cooks [a,*]

[a] Department of Chemistry, Purdue University, 560 Oval Dr., West Lafayette, IN 47907 (USA)

[b] Birck Nanotechnology Center, Purdue University, 1205 W State St., West Lafayette, IN 47907

Email: cooks@purdue.edu

Table of Contents

Chemicals. Liquid chromatography-MS-grade water (Fisher Scientific) was utilized for all experiments. AR ACS 36.5-38% formaldehyde solution was purchased from Macron Fine Chemicals and prepared at 3.65-3.8% (v/v) in LCMS-grade water unless otherwise noted. LiBr, $LiClO_4$, LiOH, NaBr, and KBr were all of ≥ 99% purity, purchased from Sigma-Aldrich, and were prepared at a final concentration of 100 mM for all experiments unless otherwise noted. Hexamethylenetetramine (hexamine) (≥99%), Hexamethylenetetramine-$^{13}C_6$, $^{15}N_4$ (99 atom% ^{13}C, 98 atom% ^{15}N, overall purity ≥99%) and graphite foil (0.5mm thickness, flexible graphite, 99.8%) were also purchased from Sigma-Aldrich. High purity compressed N_2 and Ar gases (≥99.95%) were purchased from Indiana Oxygen. The same compressed N_2 cylinder was utilized for all experiments in which an N_2 sheath gas was supplied. ^{15}N-labeled N_2 (≥99.8 atom% ^{15}N, ≥99%) was purchased from Sigma-Aldrich. Laboratory air was compressed using a 6-gallon oil-free pancake air compressor (Porter-Cable). All reagents and solvents were used as received.

(Electro)spray Deposition and Ionization. Nano-electrospray ionization (nESI) capillaries were made from borosilicate glass capillaries (Sutter Instrument Co. outer diameter 1.5 mm, inner diameter 0.86 mm) and pulled to ca. 5 µm outer diameter via a Flaming/Brown micropipette puller (P-97, Sutter Instrument Co.). Samples analyzed by mass spectrometry (MS) were ionized with a +2 kV spray potential, which was supplied directly by the mass spectrometer to a stainless-steel electrode placed inside the nESI capillary. nESI capillary were held approximately 5 mm away from the inlet of the mass spectrometer to limit the extent of any additional accelerated chemistry in the microdroplets, as is routine practice. The electrosonic spray ionization (ESSI) apparatus (used for both electrospray deposition (ESD) and other spray deposition experiments) was constructed with 100-µm inner diameter fused silica capillary (PolyMicro). The fused silica capillary was connected one on end to a 1 mL gastight syringe (Hamilton Robotics) via two nanotight sleeves, two gastight ferrules, and a union assembly to establish a flow of solution. The liquid flow was joined with the sheath gas at a tee assembly with another nanotight sleeve and gastight ferrule (all sleeves and unions purchased from IDEX Health and Sciences). Solutions were flowed at a rate of 25 µL/min via an infuse syringe pump (Standard Infusion PHD 22/2000, Harvard Apparatus). Nebulizing gases flowed at a rate of 5 L/min with a backing pressure of 100 psi. For reactions incorporating ^{15}N into hexamine, ^{15}N-labeled N_2 was diluted to 10% by volume with a stream of 99.995% purity N_2. The distance from the fused silica capillary outlet and the deposition surface was maintained at 7-9 cm to allow complete or nearly complete de-solvation of microdroplets prior to contacting the surface. Deposition experiments which utilized an external potential were performed for 20 minutes whereas those without an applied potential were

performed for 60 minutes. When utilized, high voltage was applied to the metal syringe needle and graphite surface via alligator clips (Associated Research) supplied by a Finnigan MAT Bertan DISIMS Reversible Power Supply connected to line power. The live (+) wire was applied to the metal syringe needle and the ground (-) wire to the graphite surface. The measured output during ESD experiments was *ca.* +3.7 kV. In experiments performed without an applied voltage, the deposition surfaces were grounded to minimize surface charging from impinging droplets and/or contact electrification. All surfaces were washed by pipetting and re-pipetting 500 µL of LCMS-grade water until all residue appeared to be removed.

Mass Spectrometry. Low-resolution mass spectra and ion trap collision-induced dissociation (IT-CID) were recorded on a LTQ XL ion trap mass spectrometer (Thermo Scientific) and high-resolution mass spectra were collected using an LTQ Orbitrap XL mass spectrometer (Thermo Scientific), both using the ionization parameters described above. Helium was used as the bath gas for both instruments. The inlet capillary temperature was held at 225 C and both the capillary (15 V) and tube lens voltages (65 V) were optimized to minimize any potential in-source fragmentation or associated reactivity. For all tandem mass spectrometry (MS/MS) experiments, precursor ions were isolated using a ± 1.5 *m/z* window and activated at 30 CID energy (instrument manufacturer reference values) with an activation time of 30 ms. Due to its increased stability, the lithium-adducted diethylene glycol monoethyl ether contaminant at *m/z* 141 was subject to CID at a nominal 40 energy. The maximum ion injection time was set to 100 ms for all MS and MS/MS experiments. All full scan and product ion mass spectra represent at least 15 averaged scans.

Desorption Electrospray Ionization - Mass Spectrometry (DESI-MS) Imaging. Mass spectrometry imaging experiments were carried out using a Waters Synapt G2-Si quadrupole time-of-flight mass spectrometer equipped with a 2D DESI stage, an XS-generation DESI sprayer, and a prototype heated transfer capillary (Waters Corporation). DESI was carried out using MS-grade methanol as spray solvent (2 µL/min), a spray voltage of 0.7 kV, and nitrogen as nebulizing gas (27 psi). The temperature of the heated transfer capillary and the instrument source were set at 450 °C and 150 °C, respectively. Mass analysis was carried out in the positive ion mode (*m/z* 100-200) using the sensitivity acquisition mode of the instrument. Imaging experiments were performed at a resolution of 200 x 200 µm with a scan rate of 800 µm per second for a scan time of ca. 0.25 seconds. Waters HDI software was utilized for experiment definition, data processing and analysis. Note that there is a constraint on the dimensions of the area that can be imaged in a given experiment (ca. 4,500 mm^2) which limited the area analyzed around the center of the collection surface. The individual ion images shown correspond to the relative intensity

(normalized to the total ion current) of a specific *m/z* for each pixel after application of linear interpolation smoothing. Figures 3B and 3C were collected with a resolution of 350 x 350 μm while 3D and 3E have a resolution of 200 x 200 μm.

Transmission Electron Microscopy - Energy Dispersive X-Ray Spectroscopy (TEM-EDS). Nanoparticle (NP) samples were prepared by electrospray deposition of 10 mM aqueous LiBr with 3.7% formaldehyde for 15 minutes onto Cu TEM mesh grids (CF400-Cu, Electron Microscopy Science) which were used as landing surfaces. TEM grids were placed atop a grounded graphite sheet during the deposition process. TEM investigation and EDS analyses on the NP samples were performed with a Thermo Fisher Scientific Talos 200i TEM microscope operated at 200 kV equipped with a high-angle annular dark field (HAADF) detector and SuperX EDS with four silicon drift detectors. NP size analysis was performed using ImageJ software (National Institutes of Health) with the aforementioned TEM images as the input data and data was fit to a Gaussian distribution in Origin 2025 (OriginLab).

Electron Energy Loss Spectroscopy (EELS). A Thermo Fisher Scientific Themis Z microscope operated at 300 kV was used for direct electron energy-loss spectroscopy (EELS) analyses of Li and O K-edge structures of the nanoparticles formed from electrolytically deposited aqueous LiBr/HCHO solutions. The microscope is equipped with an electron energy monochromator, a fifth-order probe spherical aberration corrector, a high-angle annular dark field (HAADF) detector, and SuperX EDS with four silicon drift detectors. EELS analyses were carried out on a Gatan Quantum 965 spectrometer to probe the lithium and oxygen K edge structures under STEM mode with the following optical parameters: an electron probe size of 0.090 nm, a convergence semi-angle of 17.9 mrad, collection semi-angle of 5.75 mrad, energy dispersion of 0.25 eV/channel, and a dwell time of 0.5 s. Measurements were collected in dual EELS mode to collect data on the zero-loss peak (ZLP), low-loss, and high-loss energy regions. ZLP alignment was performed after the scan to compensate for ZLP drifting during the scan. Spectral images were collected on areas of interest (containing visible nanoparticles) with a pixel size of 26x26 nm. All EELS scans were collected under drift correction mode.

Mass Spectrometric Quantitation of NH_3 and Hexamine. A calibration curve was constructed by first electrospray depositing a solution of *ca.* 3.7% formaldehyde solution containing 100 mM of LiBr using an Ar sheath gas with the gas and liquid flow rates described above. Ar was used to prevent the formation of hexamine via the Li_3N intermediate. The dry surface was then thoroughly washed with 500 μL of an aqueous solution containing 500 μM hexamine-$^{13}C_6$,$^{15}N_4$ and unlabeled

hexamine with varying concentrations of 125, 62.5, 31.3, or 15.6 μM; this solution was analyzed by nESI-MS. Both protonated hexamine (*m/z* 141) and protonated labeled hexamine (*m/z* 151) were simultaneously isolated using a wide isolation window of 12 *m/z* width centered about nominal *m/z* 146 and then subject to 30 CID energy. This approach enabled simultaneous ratiometric quantitation of hexamine concentration via the diagnostic product ions at *m/z* 112 (hexamine) and at *m/z* 120 (labeled hexamine) in addition to determination of any isobaric DEGMEE contaminant (nominal precursor *m/z* 141) via its diagnostic product ion at *m/z* 123. This process was repeated in triplicate for each of the four unlabeled hexamine concentrations to establish average values and error bars for each data point on the calibration curve (± 1 standard deviation about the mean). We note that the average value for these data points did not differ significantly whether an external potential was applied or not during the initial deposition process where no hexamine is expected to be formed. The calibration curve presented in the paper (Figure 3A) was constructed with data points collected from true electrospray deposition experiments (potential applied). The R^2 value(s) and equation for the linear line of best fit with propagated error as calculated in Origin 2025 was found to be:

$$y = (0.00138 \pm 0.00002)x - (0.00141 \pm 0.0028)$$

Equation	y = a + b*x
Plot	B
Weight	Instrumental (=1/ei^2)
Intercept	0.00141 ± 0.00237
Slope	0.00138 ± 1.97714E-5
Residual Sum of Squares	0.15332
Pearson's r	0.99979
R-Square (COD)	0.99959
Adj. R-Square	0.99938

Following 20 minutes (applied external potential) or 60 minutes (no applied potential) of depositing a ca. 3.7% formaldehyde solution containing 100 mM of LiBr using the gas and liquid flow rates described above and a pure N_2 sheath gas, the surface was washed with 500 μL of an aqueous solution of 500 μM hexamethylenetetramine-$^{13}C_6$, $^{15}N_4$. This solution was then analyzed via the wide isolation MS/MS method mentioned above and the resulting ratio of diagnostic product ion peaks was used with the linear equation of best fit to determine the concentration of synthesized authentic hexamine. These two experiments were repeated in triplicate, yielding a rate of NH_3 production of 2.97 ± 0.36 μg NH_3/hour/sprayer when an external potential was applied and 320 ± 220 ng NH_3/hour/sprayer without applied voltage, following basic stoichiometric conversions from the interpolated average concentration of authentic hexamine (x-axis of

calibration curve). Note that the no voltage case falls between the limit of quantitation and limit of detection and thus cannot be directly compared to the case with the application of HV.

Bubbling Control Experiments. Control experiments were performed by bubbling N_2, Ar, or compressed laboratory air (collected inside or outside the fume hood) at a rate of 500 mL/min through a 500 µL solution of aqueous formaldehyde (ca. 3.7% (v/v)) and 100 mM LiBr for 200 minutes. The chosen gas flow rate was 10x less than that utilized in spray deposition experiments in order to minimize violent bubbling and the introduction of additional air-water interfaces. The time for bubbling was adjusted accordingly. Reactions were performed in 20 mL glass scintillation vials (ALWSCI) that were initially washed with LCMS-grade water, acetonitrile, and 2-propanol (then dried at 65 C for 1 hour) prior to addition of the formaldehyde/LiBr solution. A gas line was fed into the solution through the septum cap of the vial along with another equal size gas exhaust line. After the bubbling experiments were completed, the solutions were directly analyzed by nESI-MS.

Drop Cast/Thin Film Control Experiments. Drop cast control reactions were performed by depositing 500 µL of either pure water, ca. 3.7% formaldehyde solution, 100 mM aqueous LiBr, or a combined aqueous solution of ca. 3.7% formaldehyde and 100 mM LiBr through the standard ESD setup previously described at a flow rate of 250 µL/min and without an applied sheath gas. These solutions were spread into thin films across a graphite surface via plastic weighing spatulas and placed in a fume hood with an N_2 gas flow applied to the thin films from above. This was performed in an attempt to replicate the experimental conditions used in the (electro)spray deposition experiments but with the contribution of droplet chemistry and droplet deposition removed. Solutions were allowed to dry to completion (3 hours). Each drop cast thin film area was washed with 50 µL of LCMS-grade water and analyzed by nESI-MS to determine the presence of any hexamine product. None of the drop cast experiments showed any evidence of hexamine formation in the full scan or product ion mass spectra regardless of the solution utilized or the application of an external potential, thus emphasizing the impact of microdroplet chemistry and droplet deposition on Li-mediated N_2 reduction.

Table S1. HRMS analysis of the solution collected following ESD with $^{15}N_2$ gas diluted into the $^{14}N_2$ sheath gas stream (10% (v/v)). The table represents all peaks with a signal-to-noise ratio greater than 3 which lie between nominal *m/z* 141-146.

Nominal *m/z*	Formula	Theoretical *m/z*	Measured *m/z*	Error (ppm)	Relative Intensity (%)
***m/z* 141**	$C_6H_{13}N_4^+$	141.1135	141.1132	-1.93	100
***m/z* 142**	$C_6H_{13}N_3{}^{15}N^+$	142.1105	142.1108	2.05	0.32
***m/z* 142**	$C_5{}^{13}CH_{13}N_4^+$	142.1168	142.1163	-3.72	7.9
***m/z* 143**	$C_6H_{13}N_2{}^{15}N_2^+$	143.1075	143.1138	17.3*	0.14*
***m/z* 143**	$C_5{}^{13}CH_{13}N_3{}^{15}N$	143.1139	143.1138	-0.57	0.09
***m/z* 143**	$C_4{}^{13}C_2H_{13}N$	143.1202	143.1207	3.89	0.11
***m/z* 144**	$C_6H_{13}N^{15}N_3^+$	144.1046	144.1042	-2.55	0.13
***m/z* 145**	$C_6H_{13}{}^{15}N_4^+$	145.1016	145.1012	-3.18	6.6**
***m/z* 146**	$C_5{}^{13}CH_{13}{}^{15}N_4^+$	146.1050	146.1046	-2.58	0.07

All peaks with theoretical formulae corresponding to ^{15}N-substituted products fall within the 5-ppm mass error cutoff with the exception of certain peaks detected around *m/z* 143.11-143.12.

*Select scans show a peak at *m/z* 143 that falls within 5 ppm error of the theoretical *m/z* value for $C_6H_{13}N_2{}^{15}N_2^+$, though any average of 3+ consecutive scans does not. The two peaks that arise near this *m/z* value at *m/z* 143.1138 and *m/z* 142.1207 likely correspond to the ^{13}C isotope of $C_6H_{13}N_3{}^{15}N^+$ and the $^{13}C_2$ isotope of $C_6H_{13}N_4^+$, respectively.

** An unknown isobaric contaminant is present and inflates the RI value of the peak at *m/z* 145.1012. This is further addressed in Figure S4.

Table S2. Baseline-corrected relative intensities and errors for hexamine and related species peaks at *m/z* 141-145 when unlabeled N_2 is used as a sheath gas *vs.* when $^{15}N_2$ is used. Data was collected on a low-resolution ion trap mass spectrometer. One can observe that the relative intensities (and errors compared to the expected RI values) are greater for all peaks above *m/z* 141 when labeled N_2 is used than when it is not, indicating the presence of ^{15}N-incorporation into the hexamine products. For *m/z* 142 and *m/z* 143, the RI errors are approximately one order of magnitude greater when labeled N_2 was utilized. The dramatic *ca.* 2000% error present for the trisubstituted peak is likely due to the peak intensity being near to the signal-to-noise threshold and the extremely low theoretical peak RI. While the tetrasubstituted species peak at *m/z* 145 falls below the signal-to-noise cutoff of 3, peak isolation reduced chemical noise and enabled a greater degree of sensitivity thereby facilitating an MS/MS spectrum to be collected (Figure 2C).

	Theoretical Peak RI	**Hexamine Peak RI using $^{14}N_2$**	**Deviation from Expected Hexamine RI when using $^{14}N_2$ (%)**	**Tetrasubstituted ^{15}N Hexamine Peak RI**	**Deviation from Expected Hexamine RI when using $^{15}N_2$ (%)***
***m/z* 141**	100	100	-	100	-
***m/z* 142**	8.1	8.6	5.2	12.8	59.1
***m/z* 143**	0.3	0.4	32.7	1.4	365
***m/z* 144**	0.0061	Below SNR 3	-	0.1	1870
***m/z* 145**	-	Below SNR 3	-	Below SNR 3	-

* *i.e.* Degree of ^{15}N incorporation; compare with "Deviation from Expected Hexamine RI when using $^{14}N_2$"

Table S3. Yields of NH_3 following 20-minute (electro)spray deposition

	LiBr	$LiClO_4$	LiOH	NaBr	KBr	HCHO (aq)
ESD (HV)	2.97 ± 0.36	2.5[#]	*	-	-	-
SD (no HV)	0.32 ± 0.22	X	-	-	-	-
Drop cast	-	X	-	X	X	-
Bubbling (N_2)	-	X	X	X	X	-

Data collected following ESD, 3-hour drying following drop cast deposition in a fume hood, and 120-minute bulk solution bubbling across various electrolyte solutions (all 100 mM with *ca.* 3.7% HCHO (v/v)). All values are in units of μg NH_3/hour using a single spray source and gas line.

- = No detectable hexamine product
X = Analysis was not performed
* = Detectable hexamine signal but below limit of quantitation
# = Only a single measurement was made

Scheme S1. Series of electrochemical reactions proposed to occur during the electrospray deposition process.

Step 1: Lithium salt electrolysis

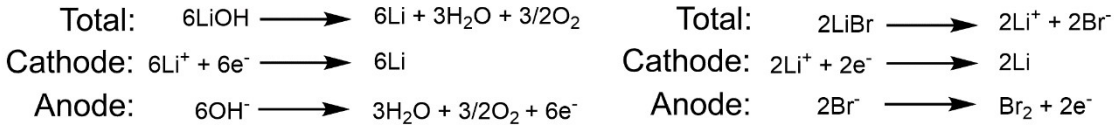

Step 2: Hydrolysis or nitridation of metallic lithium

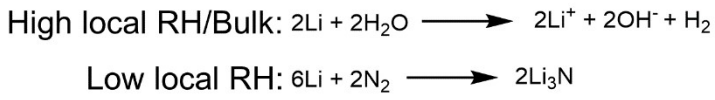

Step 3: Hydrolysis of Li_3N:

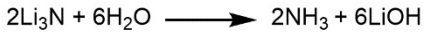

In a traditional redox reaction of an aqueous LiBr solution, water electrolysis into O_2 and H_2 would dominate given both the greater concentration and reduction potential of water (-0.83 V vs. SHE) compared to Li^+ (-3.04 V vs. SHE). Trace amounts of Li^+ would possibly be reduced at the cathode to give Li metal that would rapidly hydrolyze to give LiOH and evolve H_2, while Br^- ions would oxidize at the anode to form Br_2. This can be described as the 'high local RH/bulk' reaction in Step 2 where RH = relative humidity. However, in electrospray deposition, the impinging aqueous lithium microdroplets de-solvate during the flight from the silica capillary emitter to the deposition surface, reducing the local water concentration at the surface. This not only enables the formation of Li^+/Li nanoparticles on the deposition surface but allows the transient formation of Li_3N from N_2 provided from the sheath gas. What water does remain on the surface or in the air surrounding the nanoparticles then hydrolyzes Li_3N to form NH_3 and regenerate Li^+ as LiOH.

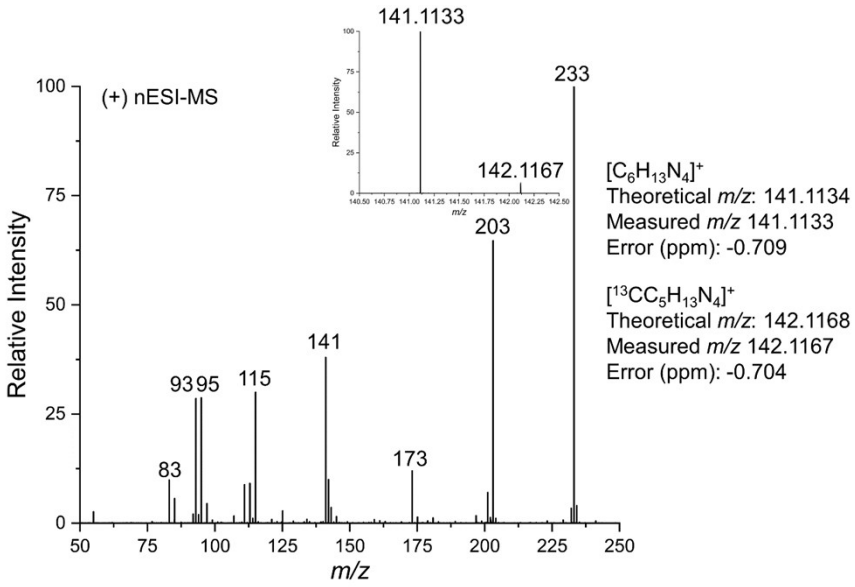

Figure S1. High-resolution full scan mass spectrum of the solution resulting from washing a graphite surface following electrospray deposition of the formaldehyde/LiBr solution described previously (Page S2). Note that this sample was diluted 2x in LCMS-grade methanol prior to nESI-MS analysis in the positive ion mode. Mass errors for both protonated hexamine and its ^{13}C isotope fall well below the 5-ppm cutoff.

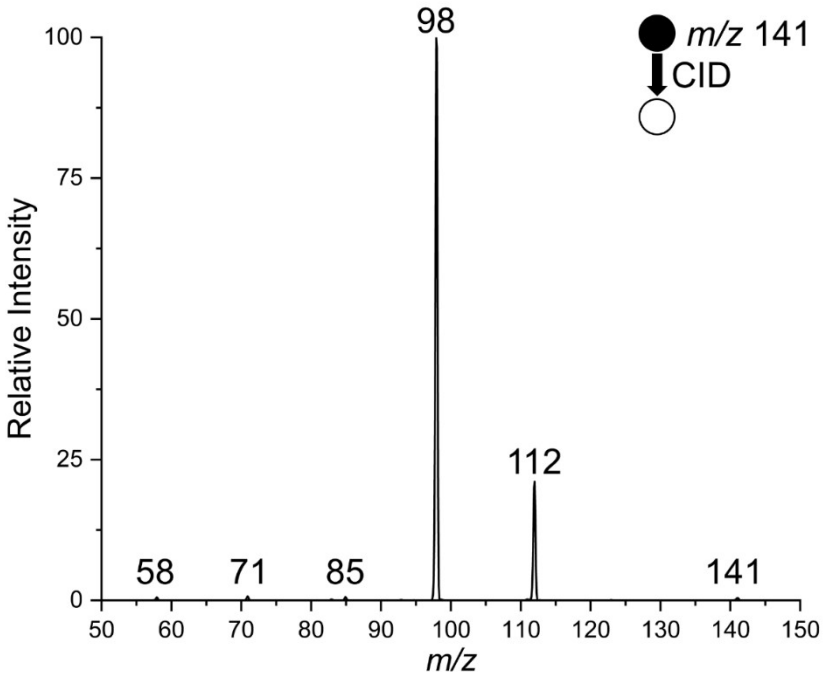

Figure S2. MS/MS of authentic hexamethylenetetramine (hexamine); $[M+H]^+$ *m/z* 141. The 1 mM aqueous sample was ionized using nESI in the positive ion mode and fragmented by CID at energy setting of 30 (manufacturer's unit). Signal-to-noise ratio for each product ion: *m/z* 58 (1957), *m/z* 71 (2690), *m/z* 85 (1941), *m/z* 98 (392132), *m/z* 112 (84026).

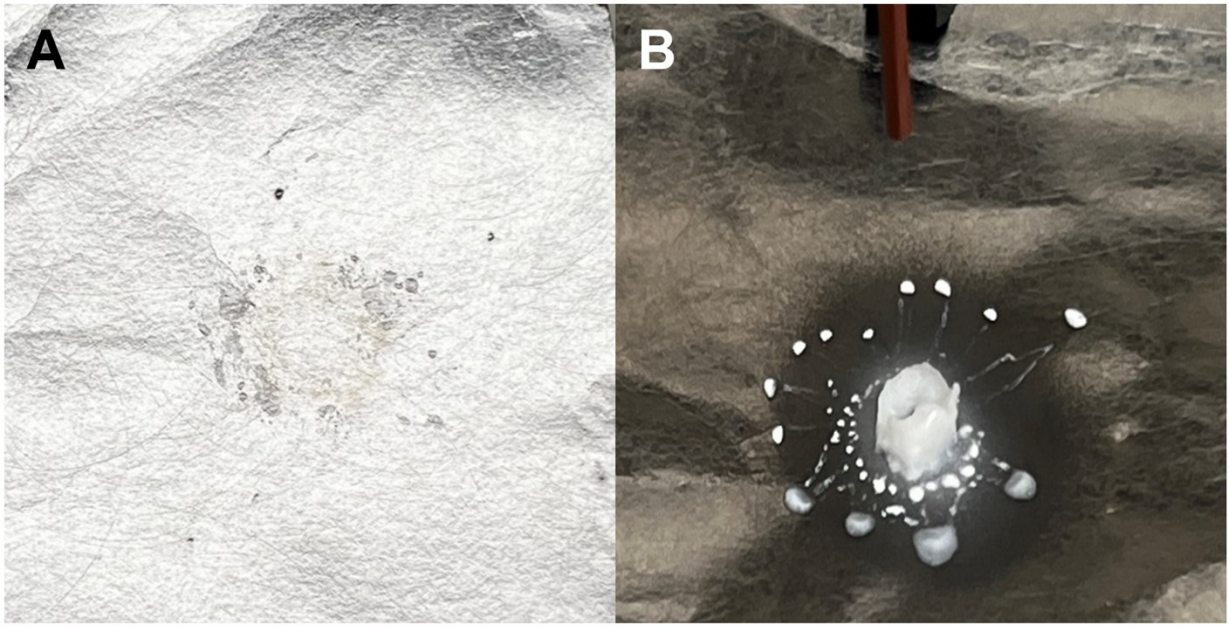

Figure S3. (**A**) Image of the graphite surface following electrosonic spray deposition of the aqueous formaldehyde/LiBr mixture for 20 minutes. White-to-silver material on the surface can be attributed to LiBr, Li_2O, paraformaldehyde, hexamine, and/or Li^0. Reddish-brown material is characteristic of Li_3N. (**B**) Hydrated paraformaldehyde structures formed following spray deposition (whether a potential was applied or not) of an aqueous formaldehyde/LiOH solution for 10 minutes. The observed structure in B is approximately 1.5 cm in diameter.

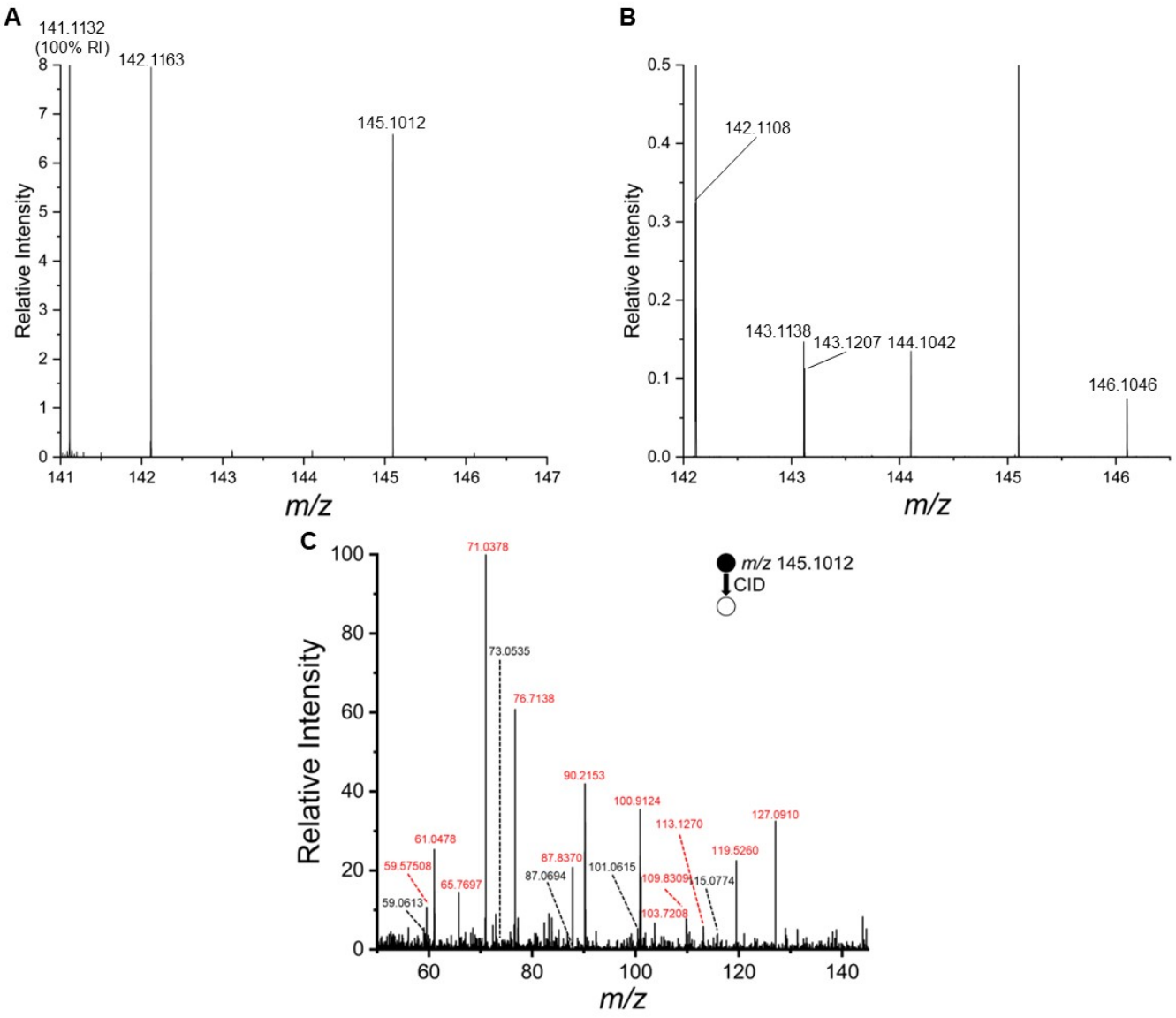

Figure S4. (**A**) Mass spectrum corresponding to Table S1 (i.e. when 10% v/v ^{15}N-labeled N_2 in unlabeled N_2 is used as the sheath gas). (**B**) Zoom-in of Figure S4A. (**C**) High-resolution MS/MS spectrum of the peak located at *m/z* 145.1012 indicating the presence of two isobaric species, one being tetrasubstituted ^{15}N-labeled hexamine (black peak labels) and the other an unknown instrument contaminant (red peak labels). Nearly all the fragments corresponding to the unknown compound are unable to be assigned a reasonable chemical formula, though some neutral loss formulae can be determined (*e.g. m/z* 127.0910 corresponds almost exactly to a loss of H_2O (18.0100 Da) from precursor ion *m/z* 145.1012).

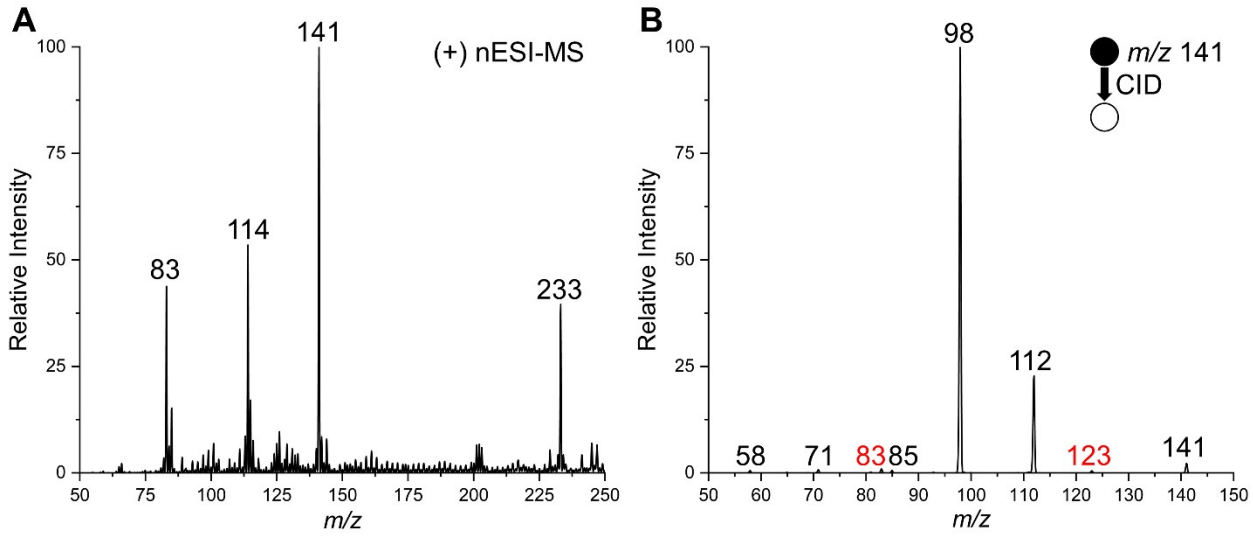

Figure S5. (**A**) Full scan mass spectrum of the solution resulting from washing a Parafilm-coated surface with water following spray deposition (with applied potential) of a formaldehyde/LiBr solution for 60 minutes. (**B**) MS/MS of the signal at *m/z* 141 at CID energy 30 primarily consists of fragments of protonated hexamine (black peak labels) with minor contributions by isobaric lithium-adducted diethyl glycol monoethyl ether as evidenced by the product ion peaks labeled in red (*see* Figure S6B).

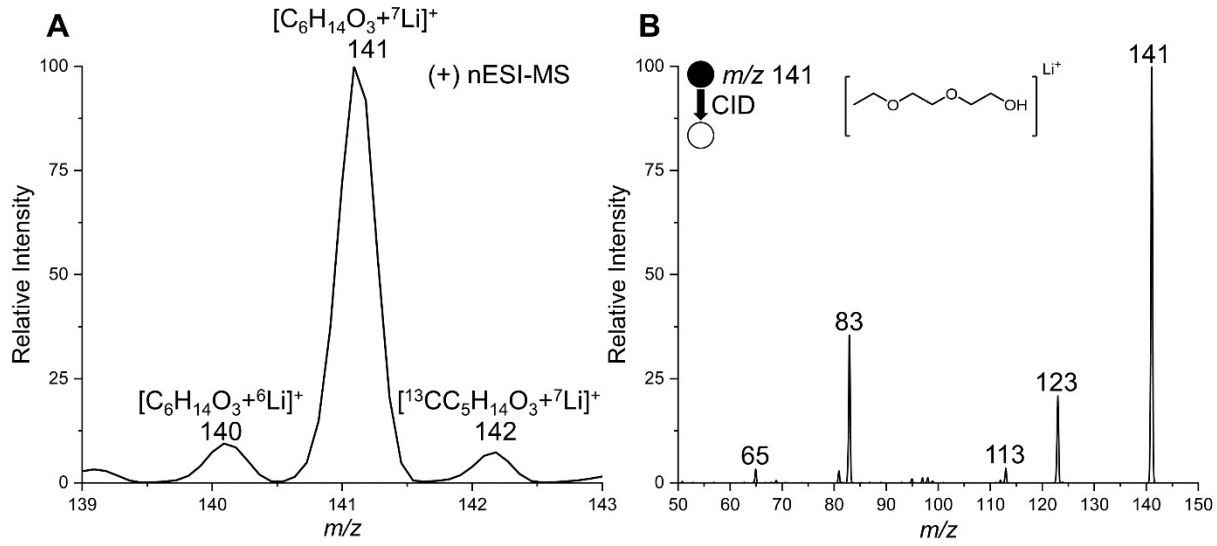

Figure S6. (**A**) Selected mass range from the full scan mass spectrum shown in Figure S9C with the peak at *m/z* 141 being assigned the formula $[C_6H_{14}O_3+^7Li]^+$, lithium-adducted diethylene glycol monoethyl ether (DEGMEE).[1] Ratios of the peak areas for *m/z* 140 (^{6}Li isotopic DEGMEE adduct), *m/z* 141 (^{7}Li isotopic DEGMEE adduct), and *m/z* 142 (^{7}Li isotopic DEGMEE adduct with ^{13}C isotope) are shown below and support the proposed chemical formula of $C_6H_{14}O_3Li^+$:

	Experimental	Theoretical	Error (%)
I_{140}:I_{141}	0.081	0.080	0.844
I_{140}:I_{142}	1.135	1.176	3.535
I_{141}:I_{142}	0.071	0.068	4.539

Peak areas were calculated by taking the area under the curve for each peak ± 0.5 *m/z* about the nominal *m/z* value. (**B**) Product ion mass spectrum for the peak at *m/z* 141 shown in Figure S5A and S9C (CID energy 30). The various product ions correspond to neutral losses of $-H_2O$ (*m/z* 123), -CO (*m/z* 113), $-C_3H_6O$ (*m/z* 83), and $–C_3H_8O_2$ (*m/z* 65).

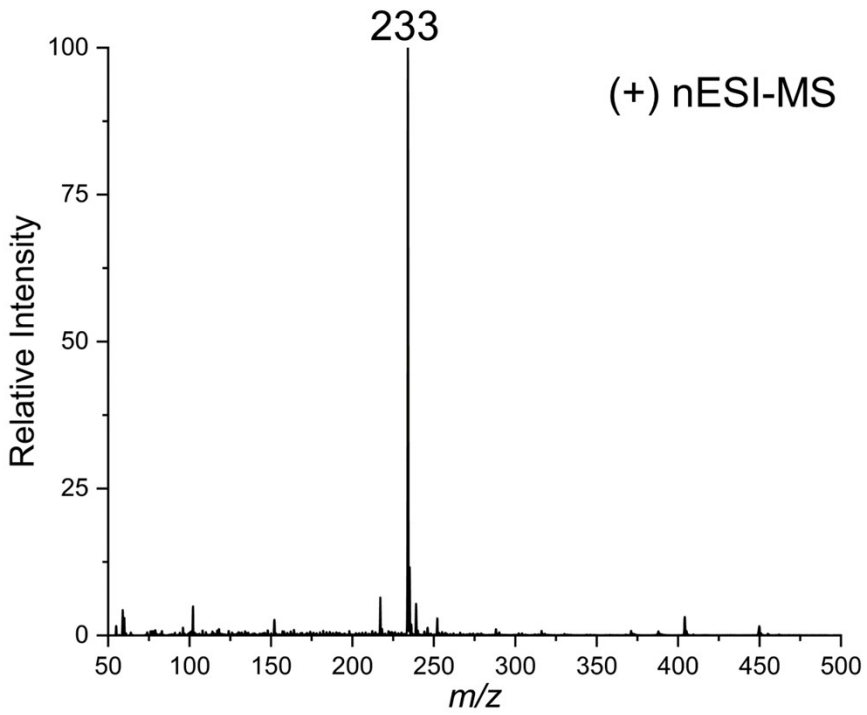

Figure S7. Full scan mass spectrum of a freshly prepared *ca.* 3.7% aqueous formaldehyde solution with 100 mM LiBr analyzed by nESI in the positive ion mode. The signal at *m/z* 233 corresponds to the lithium-adducted 8-mer of paraformaldehyde and is likely formed in solution as no other lower or higher *m/z* paraformaldehyde polymers are observed as were in the case of ESD experiments.

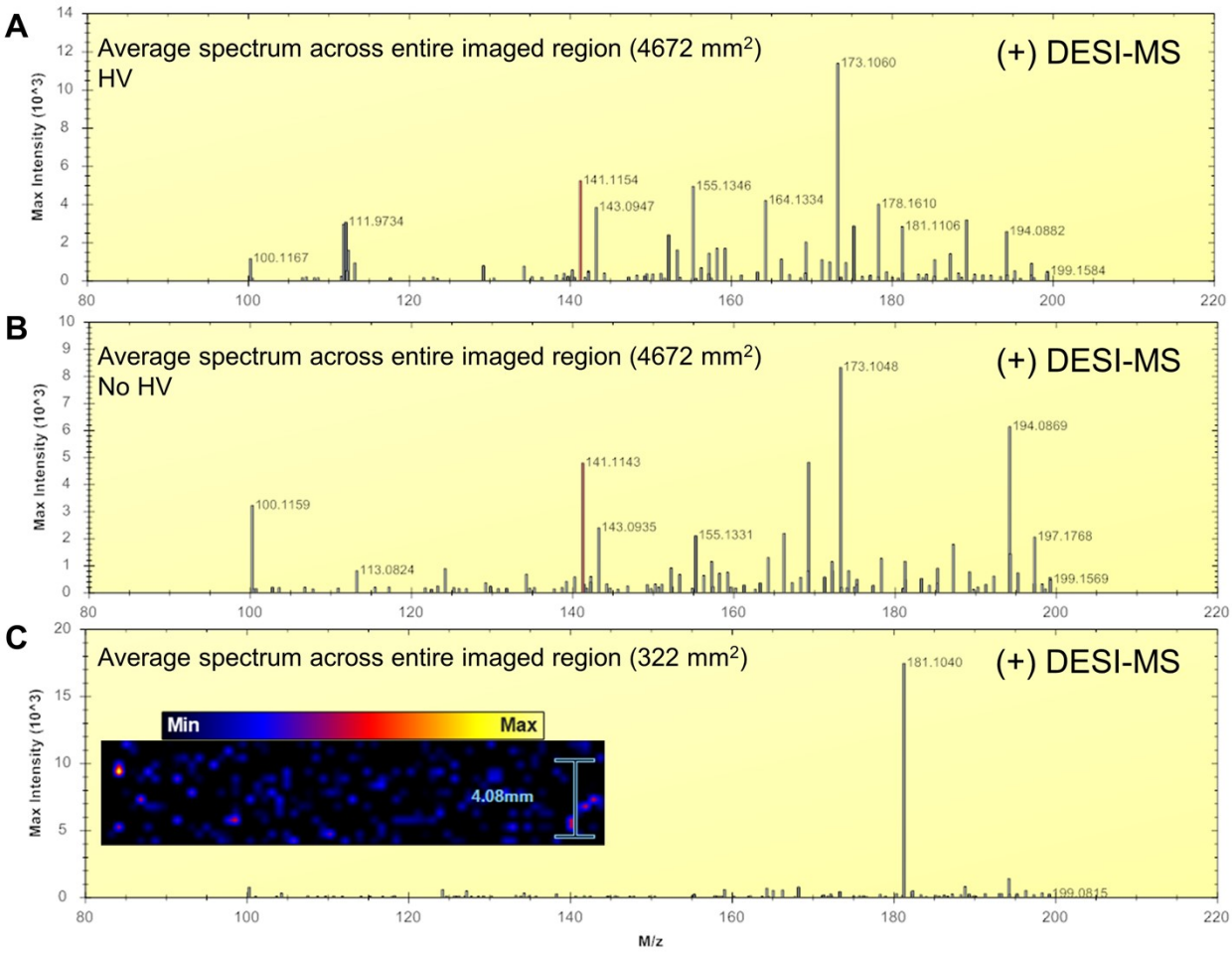

Figure S8. (**A**) Average DESI-MS full scan mass spectrum (*ca.* 112,500 individual spectra) across a 4672 mm^2 graphite deposition surface following DESI-MS imaging. High voltage was applied during the ESSI deposition of Li/HCHO. (**B**) Average DESI-MS full scan mass spectrum collected in a manner similar to that in (A) though without the application of high voltage during the ESSI deposition. (**C, inset**) DESI-MS image of a subsection of graphite foil prior to electrospray deposition and averaged spectrum (**C**). The identity of the intense peak at *m/z* 181 was not determined. It appears to be isolated to small regions of the graphite surface and the overall signal intensity is several orders of magnitude lower than that for the DESI images collected for the spray deposition experiments in Figure 3B-E (main text).

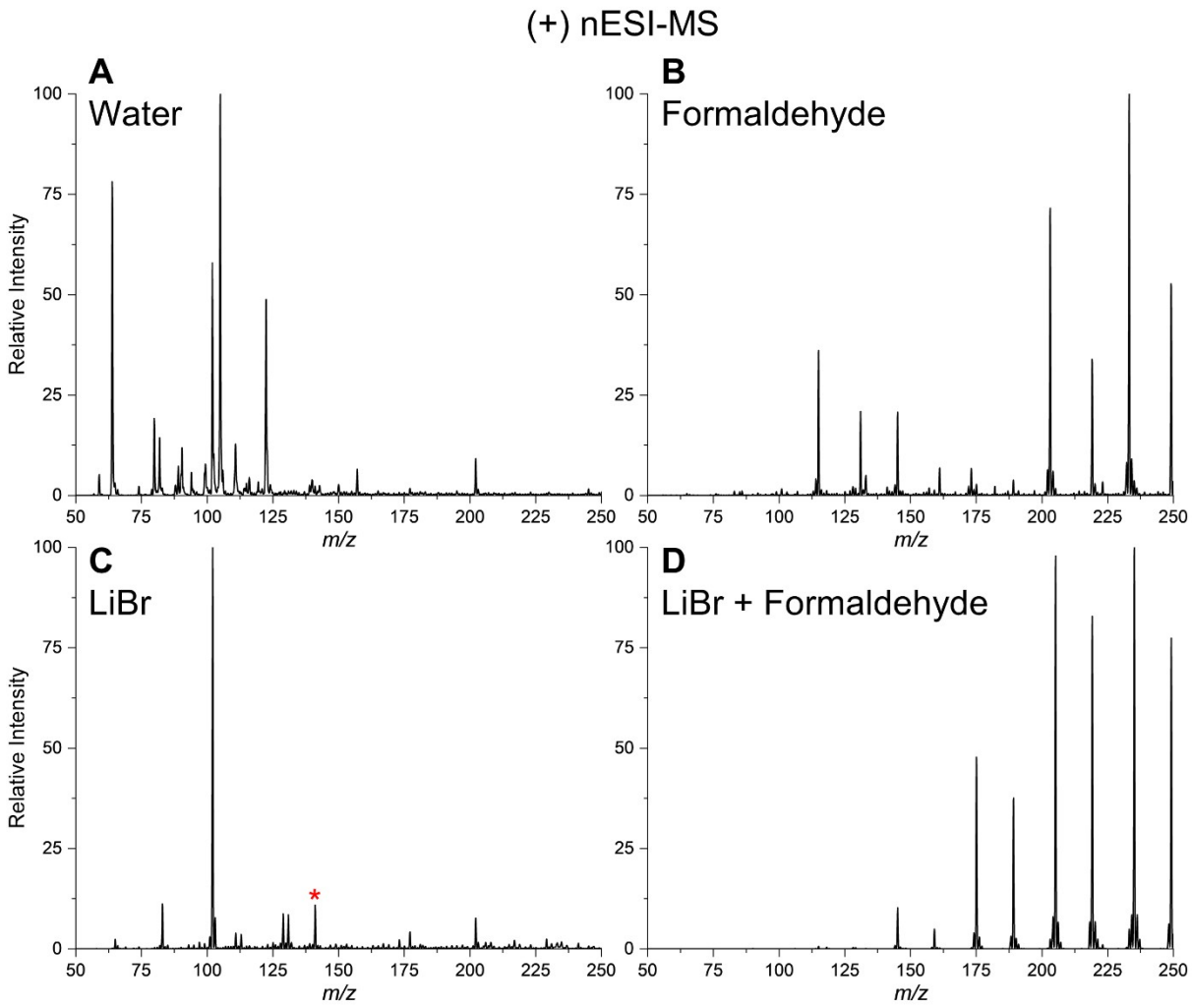

Figure S9. Full scan mass spectra of various solutions following drop cast deposition and radial spreading into thin films on an charged graphite surface with a supplemental N_2 gas flow directed from above onto the thin films: (**A**) LCMS-grade water, (**B**) *ca.* 3.7% formaldehyde solution, (**C**) 100 mM aqueous LiBr, and (**D**) the full reaction mixture of both *ca.* 3.7% formaldehyde and 100 mM LiBr. All samples were analyzed in the positive ion mode by nESI. The red asterisk in Figure S9C at *m/z* 141 corresponds to lithium-adducted diethyl glycol monoethyl ether, a ubiquitous indoor polyether contaminant, according to both full scan isotopic distributions and MS/MS analysis (Figure S6B).

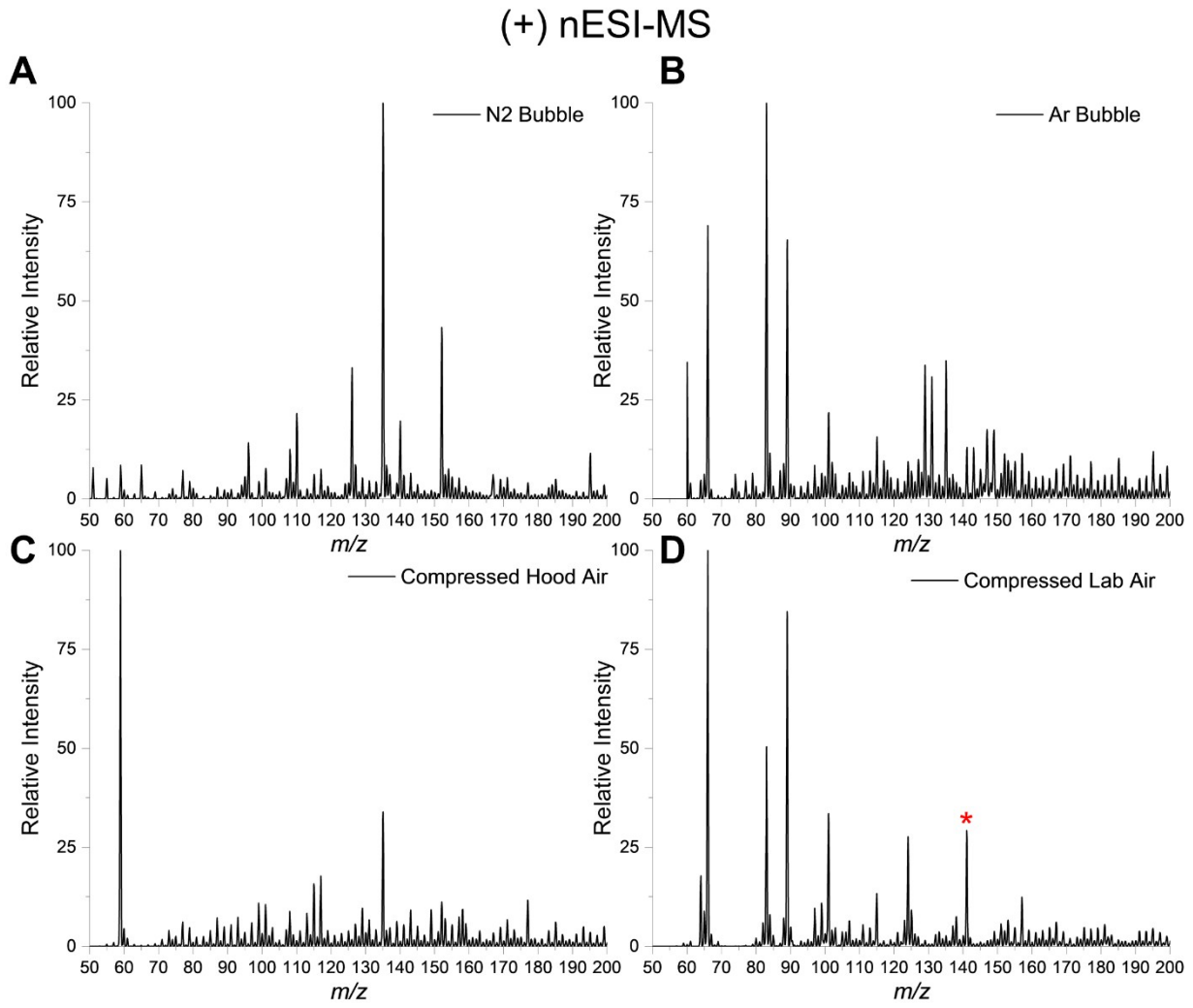

Figure S10. Full scan mass spectra of aqueous formaldehyde/LiBr solutions following bubbling of various gases: (**A**) high purity compressed N_2, (**B**) high purity compressed Ar, (**C**) compressed air from the laboratory fume hood used for all other deposition experiments, and (**D**) compressed air from the laboratory (air compressed placed outside of the fume hood). The compressed air used in Figure S10C was collected by placing the air compressor inside of the fume hood and turning it on while the sash was pulled down to the lowest working level. The red asterisk in Figure S10D corresponds to authentic hexamine, presumably formed from the reaction of ambient NH_3 with formaldehyde.

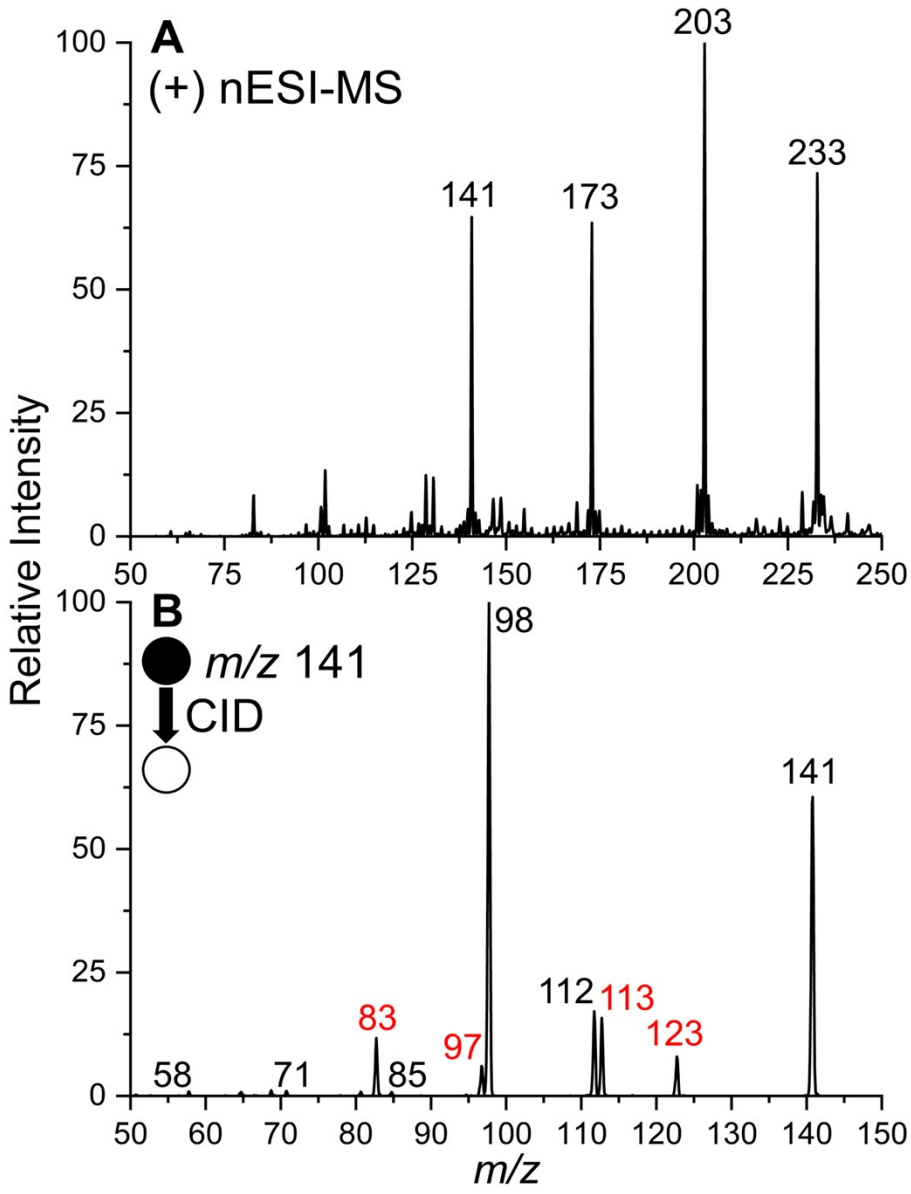

Figure S11. (**A**) Full scan mass spectrum following ESD of aqueous formaldehyde/LiBr onto a graphite surface using compressed laboratory air as the sheath gas. While a peak at *m/z* 141 is present and at a significant relative intensity, the overall signal intensity is approximately an order of magnitude lower than when pure, dry N_2 is used as the sheath gas *cf.* Figure 2A. (**B**) MS/MS spectrum of the peak at *m/z* 141 using CID energy 30 showing the presence of authentic hexamine (black peak labels), a significant amount of the Li^+-DEGMEE contaminant species is present (red peak labels).

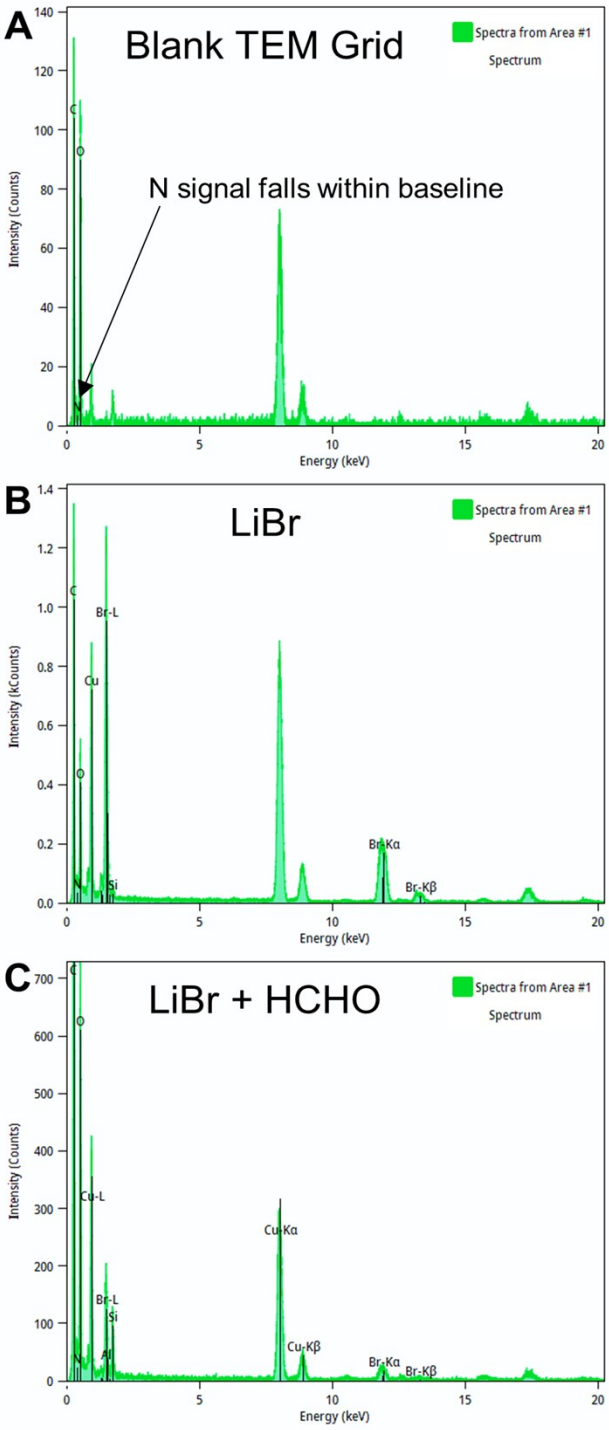

Figure S12. EDS spectra collected from a blank Formvar-coated (C- and O-containing) Cu TEM grid (**A**), LiBr solution deposited onto a TEM grid via ESD (**B**), and LiBr/HCHO solution post-ESD (**C**). The nitrogen signal is significantly enhanced in B and C compared to A, suggesting the presence of Li_3N and/or, in the case of Panel C, hexamine.

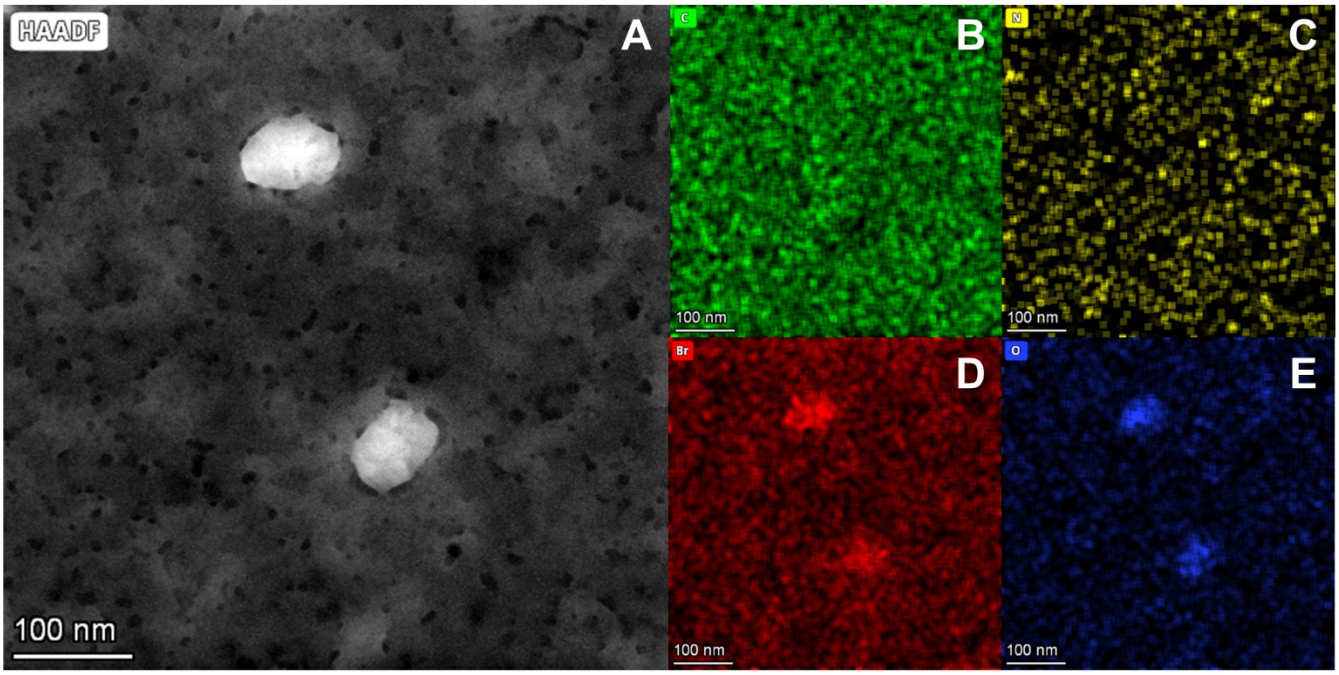

Figure S13. (**A**) High-Angle Annular Dark-Field (HAADF) STEM image of semi-cubic nanoparticles (white) and smaller nanoparticles (black) of mixed composition following ESD of an aqueous LiBr. (**B-E**) Spatial EDS elemental mappings of the deposited particles shown in Panel A with images corresponding to the distribution of carbon (**B**), nitrogen (**C**), bromine (**D**), and oxygen (**E**). The carbon signature arises from the Formvar coating on the TEM grid in addition to the deposited formaldehyde, while nitrogen is presumed to originate from Li_3N and related species.

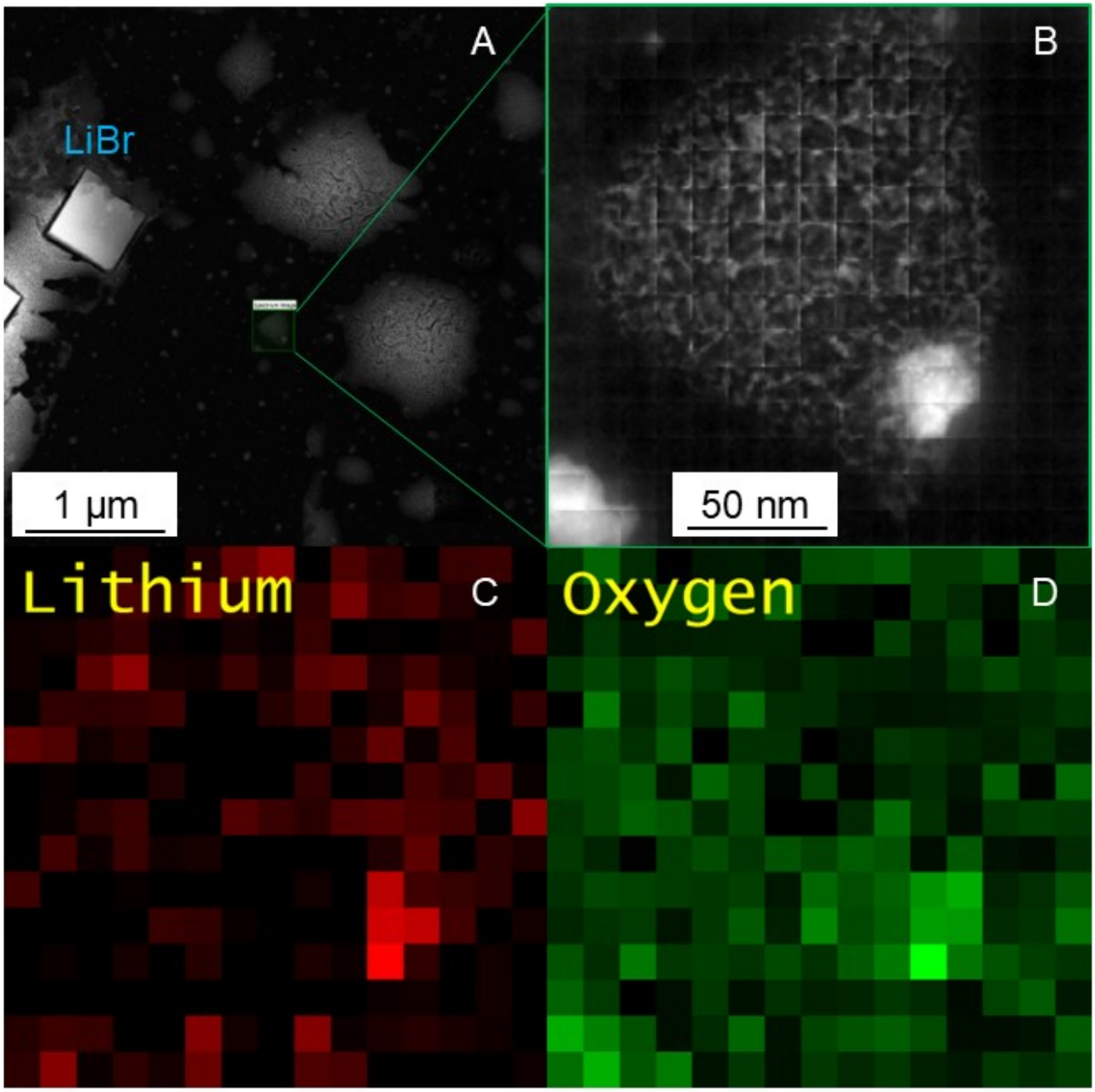

Figure S14. (A**)** HAADF STEM image showing a pristine LiBr crystal (upper left) and smaller nanoparticles encased in paraformaldehyde films (large white areas with dark fissures). (**B**) A magnified HAADF STEM image of a region (shown in A, green box) with small spheroidal NPs (faint white areas inside the larger paraformaldehyde film), along with denser and larger cubic/amorphous NPs after EELS scan. Elemental maps for lithium (**C**) and oxygen (**D**) corresponding to the area imaged in **B**. Note the greater density and co-occurrence of Li and O in the regions with the larger NPs.

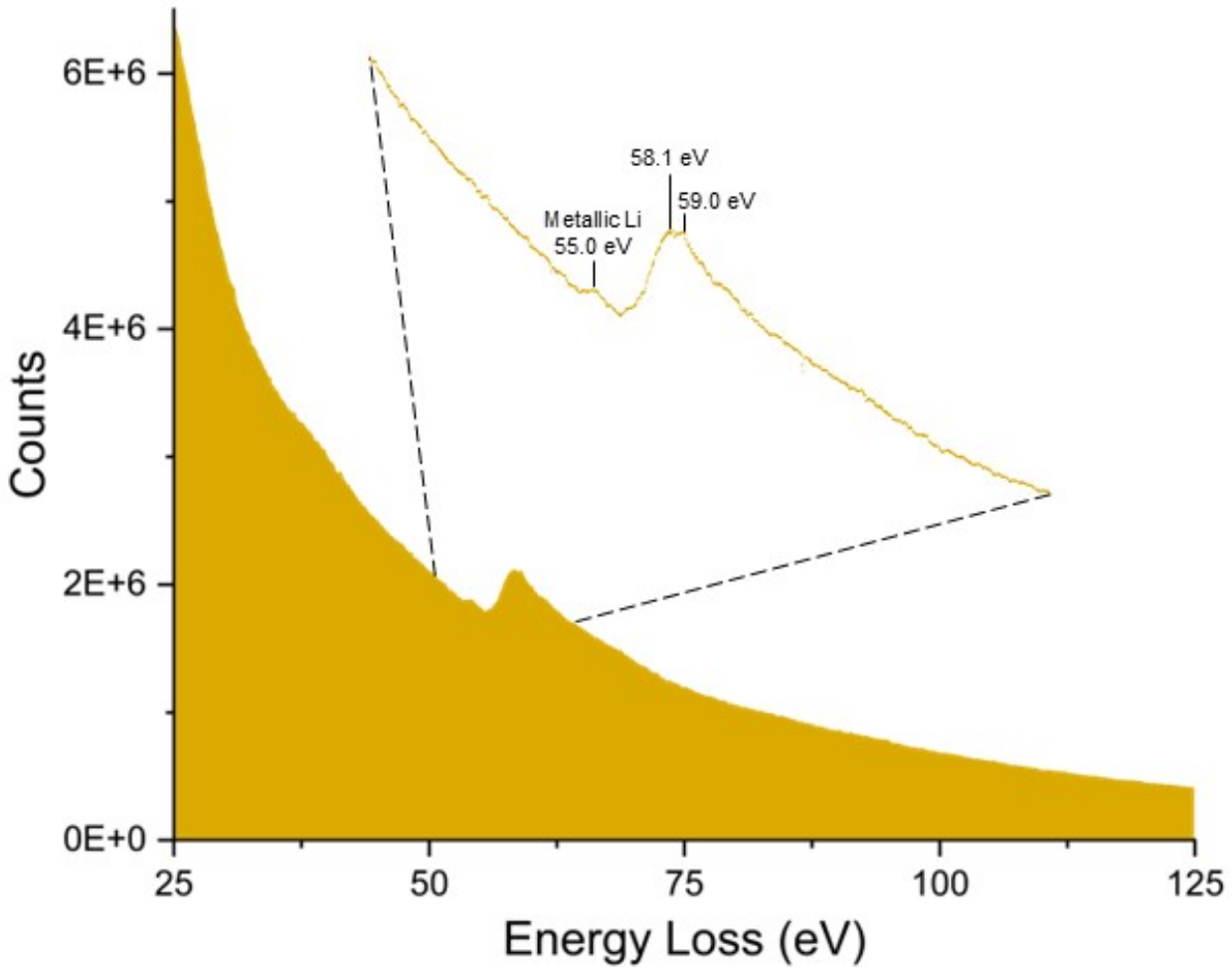

Figure S15. 14 EELS spectrum corresponding the dendritic structures shown in Figure 4A (insert, *bottom*). Signatures closely matching that of metallic Li, LiBr, and Li_2O are observed along with a raised baseline deviating from the power law-distributed plasmon peak signal.

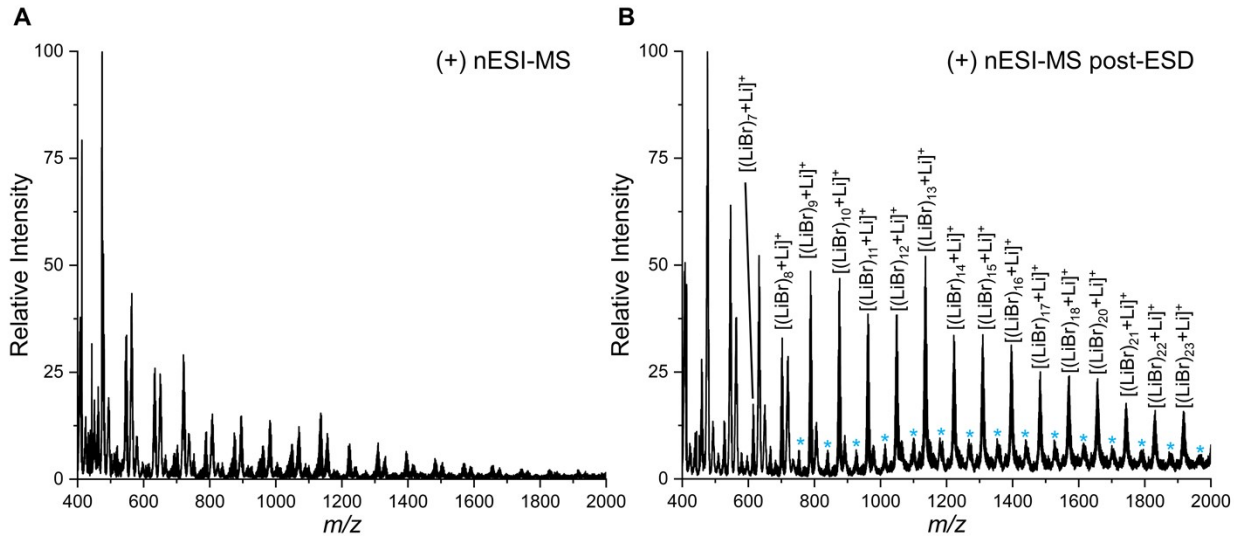

Figure S16. (**A**) Extended *m/z* region of the full scan mass spectrum for the standard LiBr and formaldehyde solution analyzed directly by nESI-MS. (**B**) The same solution after ESD (10 minutes), washing with 10 µL of H_2O, and analysis by nESI-MS showing the enhanced formation of LiBr clusters, likely precursors to the cubic nanoparticles observed via TEM in Figure 4 (inset). Additional peaks corresponding to the inclusion of 1 - 3 oxygen atoms in the LiBr clusters, as well as 1 - 3 H_2O molecules, are observed following ESD (blue asterisks; asterisks span multiple peaks), correlating well with EELS data shown in Figure S13D. As an interesting aside, the peak corresponding to $[(LiBr)_{13}+Li]^+$ is consistently more intense than other cluster peaks in the series and this trend is further exaggerated post-ESD. This peak corresponds to three complete unit cells of LiBr and hence its formation favored.[2]

Formula:

Polydispersity Index (PDI):

$PDI = (\frac{\sigma}{\bar{d}})^2$; where σ is the standard deviation of the particle size distribution and $\bar{d}$ is the mean particle diameter.[3]

References:

(1) Kumbhani, S. R.; Wingen, L. M.; Perraud, V.; Finlayson-Pitts, B. J. A Cautionary Note on the Effects of Laboratory Air Contaminants on Ambient Ionization Mass Spectrometry Measurements. *Rapid Commun. Mass Spectrom.* **2017**, *31*, 1659–1668. https://doi.org/10.1002/rcm.7951.

(2) Seifert, H. -J; Dau, E. Über Die Systeme Alkalimetallbromid/Mangan(II)-bromid. *ZAAC - J. Inorg. Gen. Chem.* **1972**, *391* (3), 302–312. https://doi.org/10.1002/zaac.19723910311.

(3) Raval, N.; Maheshwari, R.; Kalyane, D.; Youngren-Ortiz, S. R.; Chougule, M. B.; Tekade, R. K. *Importance of Physicochemical Characterization of Nanoparticles in Pharmaceutical Product Development*; Elsevier Inc., 2018. https://doi.org/10.1016/B978-0-12-817909-3.00010-8.